Environmental Pollution 287 (2021) 117602

Contents lists available at ScienceDirect

Environmental Pollution

journal homepage: www.elsevier.com/locate/envpol

Assessing the regional biogenic methanol emission from spring wheat during the growing season: A Canadian case study☆

Mengfan Cai [a], Chunjiang An [a,*], Christophe Guy [b], Chen Lu [c], Fereshteh Mafakheri [d]

[a] Department of Building, Civil and Environmental Engineering, Faculty of Engineering and Computer Science, Concordia University, Montreal, QC H3G 1M8, Canada
[b] Department of Chemical and Materials Engineering, Concordia University, Montreal, QC H3G 1M8, Canada
[c] Institute for Energy, Environment and Sustainable Communities, University of Regina, Regina, SK S4S 0A2, Canada
[d] Concordia Institute for Information Systems Engineering, Concordia University, Montreal, H3G 1M8, Canada

ARTICLE INFO

Keywords:
Biogenic methanol
Emission assessment
Spring wheat
Uncertainty and sensitivity
Climate change
Air pollutants

ABSTRACT

As a volatile organic compound existing in the atmosphere, methanol plays a key role in atmospheric chemistry due to its comparatively high abundance and long lifetime. Croplands are a significant source of biogenic methanol, but there is a lack of systematic assessment for the production and emission of methanol from crops in various phases. In this study, methanol emissions from spring wheat during the growing period were estimated using a developed emission model. The temporal and spatial variations of methanol emissions of spring wheat in a Canadian province were investigated. The averaged methanol emission of spring wheat is found to be 37.94 ± 7.5 $\mu g \cdot m^{-2} \cdot h^{-1}$, increasing from north to south and exhibiting phenological peak to valley characteristics. Moreover, cold crop districts are projected to be with higher increase in air temperature and consequent methanol emissions during 2020–2099. Furthermore, the seasonality of methanol emissions is found to be positively correlated to concentrations of CO, filterable particulate matter, and PM_{10} but negatively related to NO_2 and O_3. The uncertainty and sensitivity analysis results suggest that methanol emissions show a Gamma probabilistic distribution, and growth length, air temperature, solar radiation and leafage are the most important influencing variables. In most cases, methanol emissions increase with air temperature in the range of 3–35 °C while the excessive temperature may result in decreased methanol emissions because of inactivated enzyme activity or increased instant methanol emissions due to heat injury. Notably, induced emission might be the major source of biogenic methanol of mature leaves. The results of this study can be used to develop appropriate strategies for regional emission management of cropping systems.

1. Introduction

Methanol is typically the second-most plentiful volatile organic compound (VOC), after methane, in the remote troposphere. As the precursor of carbon monoxide (CO), formaldehyde (HCHO), and ozone (O_3), it can be related to harmful oxidant concentration and air quality deterioration in urban regions (Bachy et al., 2018; Wells et al., 2014). In less polluted rural areas, methanol can react with hydroxyl radical (•OH), reduce atmospheric oxidation capacity, and increase methane lifetime (Caravan et al., 2018). It can also act as precursor for secondary organic aerosols (SOAs) and particulate matter (PM) that scatter solar radiation and increase cloudiness as cloud condensation nuclei (CCN) (Cai et al., 2017, 2019; Shrivastava et al., 2017). Due to its plenitude and long lifetime compared to other VOCs, methanol has an important impact on air quality, human health, and climate change (Caravan et al., 2018; Mozaffar, 2017). Biogenic methanol emission from plants is a primary source of ambient methanol (accounting for 80%–89%) and it generally exceeds emissions of all other VOCs except terpenoids measured above a variety of different ecosystems (Harley et al., 2007; Heikes et al., 2002). Methanol is generally produced in plant cells through biochemical processes such as cell-wall loosening during cell expansion, tetrahydrofolate pathways, protein repair, and pectin methylesterase (PME) (Fig. S1). The methanol produced in plant cells can be stored in water and tissue and can be utilized in the plant cells through many metabolic pathways. It evaporates to the atmosphere through stomata or is oxidized by •OH radicals to form HCHO and,

☆ This paper has been recommended for acceptance by Pavlos Kassomenos.

* Corresponding author. Department of Building, Civil and Environmental Engineering, Concordia University, Montreal, QC, H3G 1M8, Canada.
E-mail address: chunjiang.an@concordia.ca (C. An).

https://doi.org/10.1016/j.envpol.2021.117602
Received 31 March 2021; Received in revised form 3 June 2021; Accepted 13 June 2021
Available online 22 June 2021

ultimately, CO_2. Methanol emission may be affected by environmental factors (e.g., light intensity and air temperature) and vegetation factors (e.g., stomatal conductance, leaf development, methanol pool size, and methylotrophs). Stresses such as hypoxia, high ozone concentration, frost, injury (e.g., cutting, insect or animal attacks), senescence, dehydration of plant leaves, and biomass burning can also cause methanol emissions (Brunner et al., 2007; Galbally and Kirstine, 2002). It has been reported that young leaves are higher emitters compared to mature leaves, and, similarly, that herbivore-attacked leaves are higher emitters than unattacked leaves (Fall and Benson, 1996; Penuelas et al., 2005). Understanding biogenic methanol emission could help better achieve the United Nations (UN) Sustainable Development Goals (SDGs) 13 that is to "take urgent action to combat climate change and its impact".

Previous estimates have focused primarily on methanol emissions from forests and grasses. For example, several studies have estimated the global biogenic methanol emission based on the empirical algorithms proposed by Guenther et al. (1995) and Galbally and Kirstine (2002). These estimates have varied considerably—from 70 to 350 $Tg \cdot yr^{-1}$—-with a mean of approximately 100 $Tg \cdot yr^{-1}$ (Harley et al., 2007; Stavrakou et al., 2011; Tie et al., 2003). Huve et al. (2007) proposed that cell wall expansion and stomatal conductance govern the dynamics of methanol emission from plants during the growing stage. Brunner et al. (2007), meanwhile, simulated the temporal methanol emissions from grasslands according to a simple parameterization of the leaf area index (LAI) and water vapor flux. However, croplands cover a significant proportion of the Earth's surface and, although they are negligible isoprene emitters, they may be a significant source of methanol (Custer and Schade, 2007). Wheat was selected for this study due to its large farming in the world —accounting for 15.1% of global cultivated area (FAO, 2018)—and because it is one of fast-growing crops and large methanol emitters (Mozaffar, 2017). Although crops such as wheat are regarded as a significant source of methanol, there is scarce information regarding its emission inventories and controlling mechanisms from a crop ecosystem in the diverse development phases (Mozaffar, 2017). A few studies have measured methanol emissions from wheat in chamber experiments or field observations. For example, Gomez et al. (2019) measured BVOC (including methanol) emissions from wheat at the plant-level using dynamic automated chambers only under the controlled weather conditions during a 7-d ripening period. Bachy et al. (2020) observed ecosystem-scale BVOC (including methanol) fluxes over a winter wheat field throughout the plant development period using an eddy covariance (EC) method without distinguishing plant and soil sources.

To date, though, no specific emission model for wheat methanol spanning the different developmental stages has been proposed. The emission model proposed in the present study, then, extends these previous empirical models for BVOC emissions to encompass this scope (Bachy et al., 2016; Guenther et al., 2012; Stavrakou et al., 2011). Some meteorological parameters, such as air temperature, precipitation, solar radiation, etc., are collected and used to investigate the crop biomass and emission activity factor. The purpose of the present research is to (1) develop an emission model to simulate temporal differences and spatial distribution of methanol emissions of spring wheat in different stages during the growing period; (2) evaluate the uncertainty and sensitivity in emission estimates; (3) quantify the effect of climate change on wheat methanol emissions; and (4) explore the relationships between biogenic methanol and air pollutants. This study seeks to fill these gaps by modeling, for the first time, methanol emissions from spring wheat in its various developmental stages. Moreover, it seeks to provide an updated method for the assessment of methanol emission from spring wheat or other crops using limited weather data. The results can be used to develop appropriate strategies for regional emission management.

2. Methods

2.1. General process of biogenic methanol emissions from spring wheat during the growing period in Saskatchewan

The Canadian prairie province of Saskatchewan has a continental climate, with temperatures and precipitation varying greatly between seasons, and has over 40% of Canada's farmland (more than 60 million acres). This province is the largest contributor (approximately 30%) to Canada's crop production, including spring wheat, which is the principal crop in Canada, accounting for around 20% of crop production (Statistics Canada, 2021). In 2018, the total spring wheat production from Saskatchewan was approximately 8.7 million tonnes, accounting for 18% of Saskatchewan's total crop production and ranked as the third contributor except for all wheat and canola (Government of Saskatchewan, 2018). The cropping area in Saskatchewan is mainly in the southern and central regions of the province. From the southeast to the northwest, the crop area is divided into 17 crop districts in our study. The seeding of spring wheat in 2018 is collected from the Government of Saskatchewan (2018). It is assumed to be evenly distributed among the crop districts, as shown in Fig. S2(a). The northern crop districts have a comparatively higher seeding area, with the largest value seen in crop district 13 (D13), while no seedings are seen in D4 and D15. The historical weather data and solar resource data are collected from Government of Canada (2016, 2018). Among the 17 crop districts, the mean (T, °C), minimum (T_{min}, °C), and maximum (T_{max}, °C) daily temperatures, global solar radiation (R_s, $Wh \cdot m^{-2}$), and mean daily wind speed at a height of 2 m (v, $m \cdot s^{-1}$) are generally found to increase when moving from the northwest to the southeast, while this trend does not hold for the mean daily precipitation (P, mm), relative humidity (RH, %), and dewpoint temperature (T_d, °C), as shown in Fig. S2(b-i).

Although crop residue decomposition and soil-related emission phenomena continue throughout the spring, summer, and autumn until the soil becomes frozen in winter (Shi et al., 2021), emissions from leaves during the growing period are considered the principal source of methanol emissions from spring wheat. The growing season is assumed to span the period from May 1, 2018, to September 17, 2018, for the purpose of the present study. According to the Saskatchewan Crop Reports (Government of Saskatchewan, 2018), although the seeding and harvesting periods vary slightly among the different crop districts, the growing period of spring wheat can be generally divided into seven stages: germination (*G*: G1-7), emergence (*E*: G8-21), tillering (*T*: G22-42), heading (*H*: G43-70), flowering (*F*: G71-91), yield formation (*YF*: G92-126) and ripening (*R*: G127-140) (Fig. 1). During the growing period, solar radiation and air temperature are generally higher in the *T*, *H*, *F* and *YF* stages than in the other stages (*S*, *E*, and *R*), while all meteorological variables are at a high level in the *T* stage.

2.2. Crop methanol emission model

BVOCs are closely related to the amount of carbon accumulating in the growing period which depends on the balance (net primary production, NPP) of photosynthesis (gross primary production, GPP) and respiration (R) (Collalti et al., 2020). Empirical models have been widely adopted to estimate BVOC emissions based on vegetation factors, emission factors, and environmental factors (Cai et al., 2021). The present study builds upon and extends these models to develop a Crop Methanol Emission Model (CMEM) to estimate the net methanol emissions from spring wheat during growth (E, μg compound$\cdot m^{-2}$ earth surface$\cdot h^{-1}$) into the atmosphere above the canopy at a specific time and location:

$$E_i = D_r \cdot \sum NPP_i \cdot \varepsilon \cdot \gamma \cdot \rho \tag{1}$$

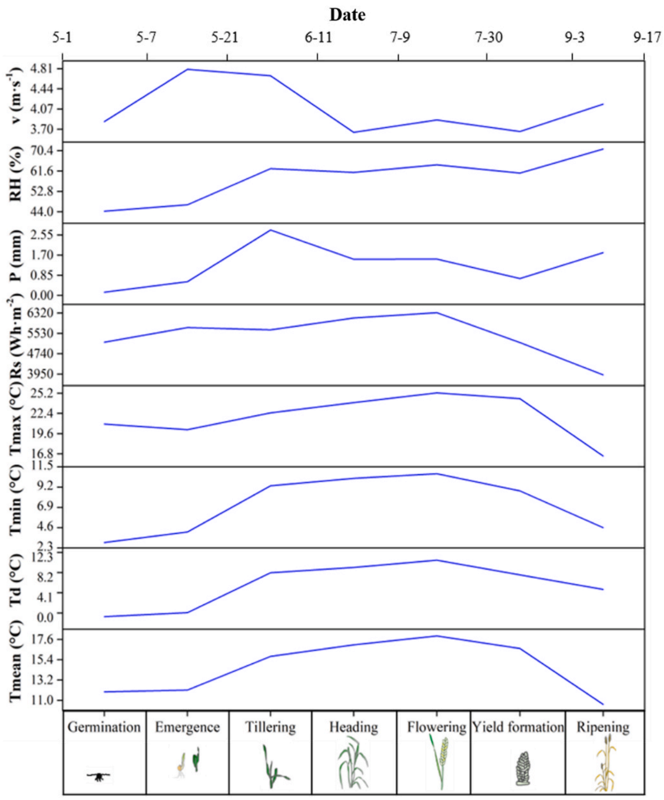

Fig. 1. Changes in meteorological variables within the spring wheat phenology.

$$NPP_i = 0.77 \times GPP = 0.77 \times PAR_i \cdot f_{PAR} \cdot LUE_{max} \cdot f_T \cdot f_W \cdot f_P \cdot f_{CO_2} \approx \frac{Yield}{HI} \tag{2}$$

$$\gamma = \gamma_{CE} \cdot \gamma_{PT} \cdot \gamma_{Age} \cdot \gamma_{SM} \cdot \gamma_{CO_2} \cdot \gamma_{Stress} \tag{3}$$

In the above equations, i represents the different growing stages of spring wheat. D_r is an ecosystem-dependent empirical coefficient and a constant value of 0.75 is selected for spring wheat that retains its foliage less than one year (Guenther et al., 1995). ε is the standard methanol emission (μg·g^{-1}·h^{-1}) into the canopy at standard conditions at a photosynthetically active radiation (PAR) flux of 1000 μmol photons·m^{-2}·s^{-1} and a leaf temperature of 303 K. Due to the lack of experimental data for standard methanol emission of spring wheat, a constant value of 1.0 μg·g^{-1}·h^{-1} is used in this model based on the dynamic methanol emissions from common wheat (*Triticum aestivum*) at the ripening stage (Gomez et al., 2019). ρ is a factor explaining the production and loss of methanol within plant canopies. It is assumed to be a constant value of 0.96 (Guenther et al., 2006).

NPP_i is the net primary production of wheat biomass in the growing period, i, in g dry matter·m^{-2}, which is estimated by the vegetation photosynthesis model (VPM). This model has been widely applied to estimate *GPP* and *NPP* of crops including wheat (Patel et al., 2010; Sánchez et al., 2015). Wheat has been found to have a constant NPP/GPP ratio over the growing period with a value of 0.77 (Albrizio and Steduto, 2003). Harvest index (*HI*), meanwhile, can be used to obtain a rough estimate of biomass using the measured grain yield of spring wheat (*Yield*, g·m^{-2}) (Bolinder et al., 2007; Dai et al., 2016). In Equation (2), *PAR* (MJ·m^{-2}) is the proportion of shortwave radiation utilized by plants for photosynthesis. f_{PAR} means a fractional interception for PAR. LUE_{max} is the maximum light use efficiency of wheat, ranging from 1.92 to 3.42 gC·MJ^{-1} (Gower et al., 1999; Sánchez et al., 2015). For the purpose of the present study, this is assumed to be a constant value of 2.55 gC·MJ^{-1}, in accordance with similar studies in North America (He et al., 2018). f_T, f_W, f_P, and f_{CO2}, meanwhile, are the LUE response to air temperature, soil moisture, phenology and CO_2, respectively. The values of f_P and f_{CO2} for spring wheat during growth are assumed to be 1. The detailed calculation for other parameters is shown in CMEM 1 in the Supplementary Material.

γ is a non-dimensional emission activity factor accounting for emission changes considering the light and temperature (γ_{PT}), soil moisture (γ_{SM}), canopy environment (γ_{CE}), leaf age (γ_{Age}), CO_2 inhibition and fertilization (γ_{CO2}), and induced stresses such as insects, fungus, and wounding (γ_{stress}). γ_{CE} and γ_{Age}, it should be noted, vary among different growing stages (Bachy et al., 2020), as shown in Table S1. γ_{CO2} and γ_{stress} are both assumed to be 1 in this study. Other detailed calculations are given in CMEM 2 in the Supplementary Material.

2.3. Uncertainty and sensitivity analysis

There is uncertainty in the estimation of both biomass and emissions. The uncertainty analysis can help obtain a better understanding of environmental processes (Asif and Chen, 2020; Ji et al., 2020; Shrestha and Wang, 2020). To determine the significant factors affecting methanol emission from spring wheat, the Monte Carlo simulations are used to assess the sensitivities and uncertainties in the emission estimate using the Crystal Ball software (v11.1.2.4) in this study. 10,000 trials are performed when each parameter is sampled independently with its respectively applicable distribution. Normal, lognormal, and uniform distributions are employed based on publicly available data and data from peer-reviewed literature (Table S2). A ±10% change is assumed when only the mean value of a variable is available. A sensitivity analysis is conducted to determine the correlation and contribution of each input variable to the methanol emissions.

However, the sensitivity analysis using the Crystal Ball software can only reveal the single effect rather than the joint effects of multiple factors. In contrast, factorial analysis has been widely applied to study the main and interaction effects of several factors on a response. In the present study, the Minitab software (v15) is adopted to conduct the design of experiments (DOE). When experimenting, two 2-level fractional factorial designs with 15 factors (128 runs) considering two situations—(1) input data and model parameters and (2) only model parameters—are conducted with DOE capabilities, respectively. The range for those factors for which data is available is set according to the literature, while a ±10% variation range is considered for those factors for which data ranges are not available (Table S2).

2.4. Quantifying the effect of climate change

Climate change has a great impact on the structure and function of ecosystems and its subsequent influences in vegetation composition will indirectly influence future BVOC emissions and composition, especially for the vegetation in cold zones (Peñuelas et al., 2013; Valolahti et al., 2015). Climate projections have been widely used for impact assessment and mitigation and adaptation measure design (Eyring et al., 2016; Wu et al., 2020). In our study, future temperature is obtained from the Coupled Model Intercomparison Project Phase 6 (CMIP6) which is an initiative of the World Climate Research Programme's Working Group of Coupled Modeling (data available at: https://esgf-node.llnl.gov/projects/esgf-llnl/). In CMIP6, a novel scenario matrix architecture combines the Representative Concentration Pathways (RCPs)—describing future greenhouse gases (GHGs) and other radiative forcings—and the Shared Socioeconomic Pathways (SSPs)—modeling future socio-economic and technological development, i.e., population, economic growth, urbanization, and education. The impacts of a changing climate on methanol emissions are assessed under two potential futures using the following SSP/RCP-based scenarios, SSP2-4.5 and SSP5-8.5. Specifically, SSP2-4.5 is a medium development (SSP2) achieving forcing levels of 4.5 W·m^{-2} while SSP5-8.5 means a high economic growth (SSP5) achieving forcing levels of 8.5 W·m^{-2}. The simulations performed using CMIP6 meteorology spanning three periods—2020–2039, 2040–2069, and 2070–2099—are compared to the methanol emissions for the year 2018 as follows:

$$RD = \frac{E_i - E_0}{E_0} \times 100\% \tag{4}$$

where *RD* (%) is the relative difference in methanol emissions between the projected periods (E_i, μg·m^{-2}·h^{-1}) and the control simulation in 2018 (E_0, μg·m^{-2}·h^{-1}) under two SSP scenarios.

Before inputting the projected temperatures into the updated emission model, a bias correction using the linear-scaling approach is conducted to correct the CMIP6 simulation temperatures as follows, as per Maraun (2016):

$$T^{i,k}_{f,corr} = T^{i,k}_{f,raw} + (\overline{T}^{i,k}_{obs} - \overline{T}^{i,k}_{contr}) \tag{5}$$

where *T* denotes daily temperature (°C); the superscripts *i* and *k* represent the different crop districts and growing stages, respectively; and the subscripts *f*, *corr*, *raw*, *contr*, and *obs* represent the future values, corrected values, raw values, modeled values in the control case, and observed values in 2018, respectively.

3. Results

The methanol emissions from spring wheat during different growing stages are estimated using the updated model for the year 2018 in Saskatchewan (Fig. 2). Over the course of the growing season, methanol emissions are found to far exceed the canopy interception and loss, resulting in positive net emissions, as shown in Fig. 2. This implies the presence of a methanol source in the agriculture ecosystem. The average methanol emission in 2018 for the various crop districts is found to be 37.94 ± 7.5 μg·m^{-2}·h^{-1}. Overall, methanol emissions are found to increase moving from north to south, with the maximum emission level, in D3 (49.08 μg·m^{-2}·h^{-1}), being about double the minimum emission level, in D17 (25.39 μg·m^{-2}·h^{-1}). As shown in Fig. 2, methanol emissions exhibit phenological peak to valley characteristics, reaching maximum emissions (100.79 μg·m^{-2}·h^{-1}) in S6 (yield formation stage) and minimum emissions (≈0 μg·m^{-2}·h^{-1}) in S1 (germination stage).

Fig. 3 shows the distribution and probability of forecast and fitted methanol emissions in terms of daily increased biomass. The average forecast emission is averaged by 10,000 simulations from Monte Carlo sampling, with a mean value of 1.11 μg·m^{-2}·h^{-1}. The uncertainty in the methanol estimation is found to be high, with a standard uncertainty of 2.07 μg·m^{-2}·h^{-1}. The methanol emissions show a Gamma probabilistic distribution, with a long tail in the high-value zone. The 95% confidence interval for the methanol emissions can be evaluated as [0, 3.18]. There is a probability of nearly 84% in the range of methanol emissions, [0, 2] μg·m^{-2}·h^{-1}, while a probability of approximately 30% in the range, [0, 0.05] μg·m^{-2}·h^{-1}.

The sensitivity results generated from the Crystal Ball software, as shown in Table S3, can preliminarily identify the key uncertainty sources in estimating methanol emissions. Growth length (*GL*), mean daily temperature (T_{mean}), activation energy (CT_1), minimum photosynthetic temperature (T_1), global solar radiation (R_s), and maximum normalized emission capacity (E_{opt}) are found to be the top six sources of uncertainties in predicting methanol emissions. To identify the primary and interactive effects of different variables on methanol emissions, 2-level fractional factorial analysis of 15 factors—selected according to the contribution of these variables to variance and rank correlation as shown in Table S3—is performed using Minitab software. Fig. 4 and Fig. 5 show two scenarios of factorial analysis considering different uncertainty sources. When input data and model parameters are included in the analysis (Fig. 4), in addition to the five most significant single factors ($SF_{p\,<\,0.05}$)—i.e., T_{mean}, GL, R_s, E_{opt}, and γ_A (leaf age factor), ten significant interactive factors ($IF_{p\,<\,0.05}$)— i.e., $T_{mean} \times GL$, $T_{mean} \times R_s$, $GL \times R_s$, $GL \times E_{opt}$, $T_{mean} \times E_{opt}$, $GL \times \gamma_A$, $T_{mean} \times \gamma_A$, T_0 (optimal photosynthetic temperature) $\times$ K (canopy extinction coefficient), CT_2 (deactivation energy) $\times$ T_1, and $T_0 \times LUE_{max}$ (maximum light use efficiency)—are found to have significant positive effects on methanol emissions. This means that several photosynthetic-related factors (i.e., T_0, T_1, K, CT_2, and LUE_{max}), although they do not have an obvious influence on the effect of $SF_{p\,<\,0.05}$ on methanol emissions, can interact to double the effect of these insignificant-single-factors ($SF_{p\,>\,0.05}$). When only model parameters are included in the analysis, more factors,

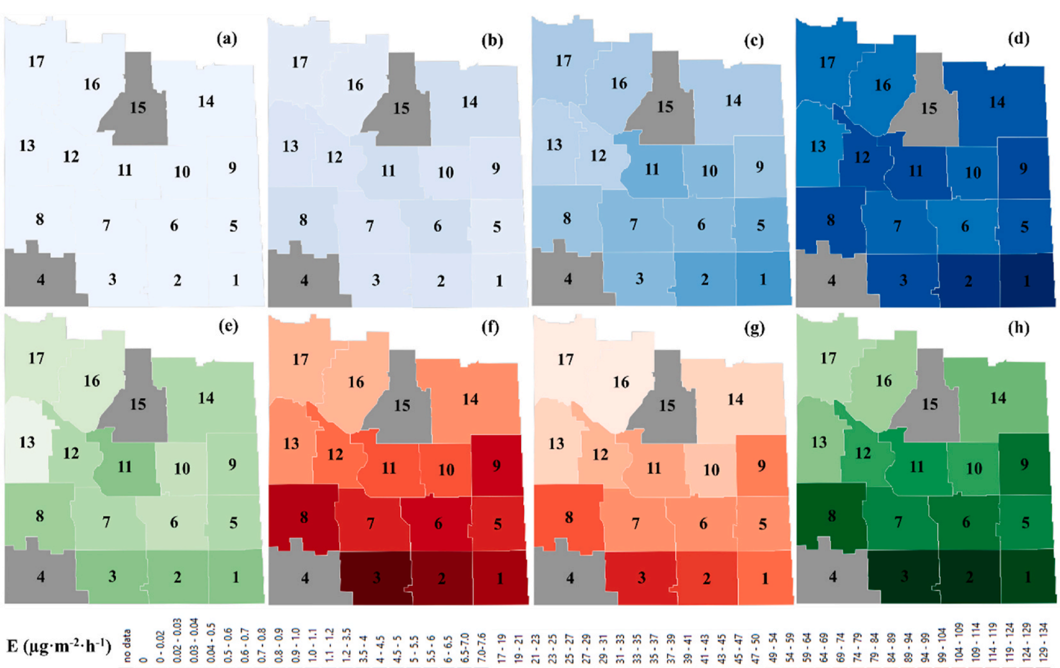

Fig. 2. Spatial-temporal biogenic methanol emissions (*E*, μg·m^{-2}·h^{-1}) among different growing stages of spring wheat in 2018. (a) Germination (*G*); (b) Emergence (*E*); (c) Tillering (*T*); (d) Heading (*H*); (e) Flowering (*F*); (f) Yield formation (*YF*); (g) Ripening (*R*); (h) Growing period (*G*).

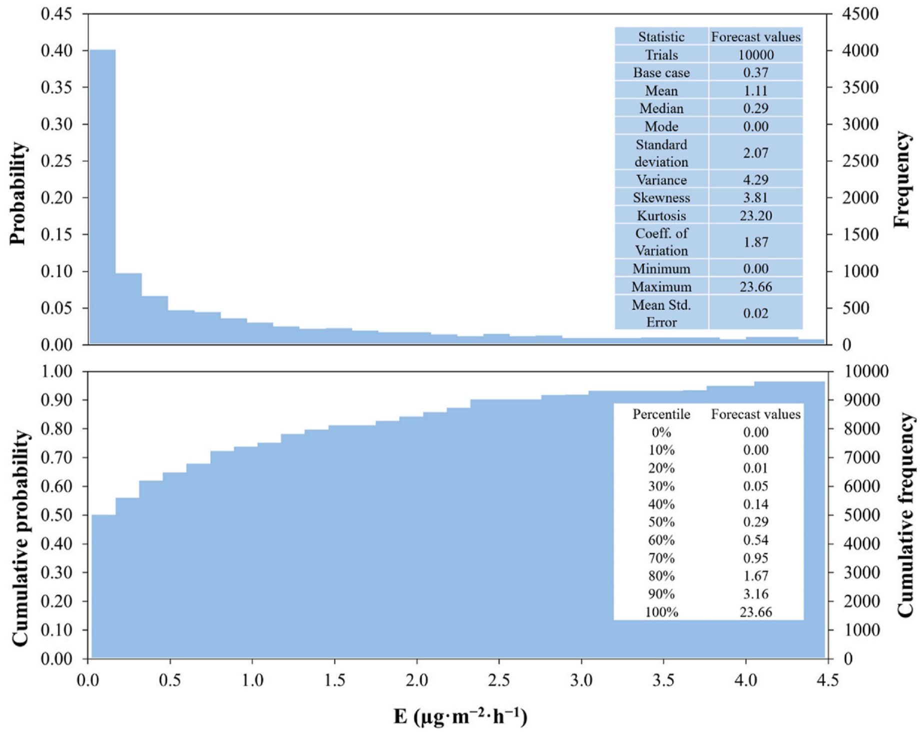

Fig. 3. Uncertainty analysis of forecast methanol emissions (E, $\mu g \cdot m^{-2} \cdot h^{-1}$) using Crystal Ball software.

including seven $SF_{p\,<\,0.05}$ and nine $IF_{p\,<\,0.05}$, are found to affect methanol emissions. Among them, K, γ_A, LUE_{max}, and E_{opt} are identified as positive SF $_{<\,0.05}$, while T_{opt} (temperature when E_{opt}), T_0, and T_1 are identified as negative $SF_{p\,<\,0.05}$, as shown in Fig. 5. Notably, the double effect of negative $SF_{p\,<\,0.05}$, including $T_{opt} \times T_0$ and $T_{opt} \times T_1$, is positive, while $IF_{p\,<\,0.05}$, such as $T_{opt} \times \gamma_A$, $T_0 \times \gamma_A$, $T_{opt} \times LUE_{max}$, and $T_{opt} \times K$, are found to be negative.

The impact of temperature change on methanol emissions according to different SSP scenarios is shown in Fig. 6. Generally, differences in methanol emissions by −35 to +25% (2020–2039), −25 to +39% (2040–2069), and −19 to +60% (2070–2099) are observed under the SSP2-4.5 scenarios, and changes of −26 to +6% (2020–2039), −38 to +34% (2040–2069), and −24 to +82% (2070–2099) under the SSP5-8.5 scenarios, compared to the control observations (year 2018) among crop districts. Moreover, the more pronounced increases are generally observed in northwestern Saskatchewan. This spatial distribution is opposite to the variations of biogenic methanol emissions for the growing period in 2018 (Fig. 2), but it is consistent with the changes in air temperatures and wheat biomass in the future scenarios (Fig. S3 and Fig. S4).

4. Discussion

4.1. Comparison with previous studies

Methanol emission of spring wheat in Saskatchewan in 2018 is found to be 37.94 ± 7.5 $\mu g \cdot m^{-2} \cdot h^{-1}$ on average (Fig. 2), much lower than the findings reported by Gomez et al. (2019) and Bachy et al. (2020). This variance may be the result of differences between stages, crop species, and measurement techniques (Table 1). For instance, chamber emissions are found to be more than fourfold higher than the EC measurements during the ripening stage (Gomez et al., 2019). Furthermore, the predicted biomass range in the present study is found to fall within the observed biomass range of common classes of wheat in North America ($HI = 0.33$ to 0.61) but to be generally lower than the observed biomass of spring wheat in Canada in particular ($HI = 0.4$), shown in Fig. 7. Moreover, spring wheat normally has a shorter growing period and yields higher biomass compared to winter wheat. Wheat biomass has a very strong relationship with methanol emissions because the two are both predominantly influenced by similar factors such as GL and T_{mean} (Table S3). Therefore, the methanol emissions from winter wheat measured by Gomez et al. (2019) are much higher than the results of

Table 1
Comparison of methanol emissions from crop and grass species.

Species	Emission[a] ($\mu g \cdot m^{-2} \cdot h^{-1}$)	Biomass[a] ($g \cdot m^{-2}$)	Climate[b]	Measuring techniques[c]	Measuring period	Reference
Spring wheat	37.94 ± 7.5 or 0–131.03	611.2 ± 50.14 or 0–689	Dfb	Model	01/05–17/09/2018 ($G \sim R$)	This study
Winter wheat	62 ± 3.3 or −459–1128	0–2000	Cfb	Field /DEC-MS/PTR-MS	05/03–July 28, 2013 ($E \sim R$)	Bachy et al. (2020)
Winter wheat	900	1000	Cfb	Chamber /In situ cuvette/PTR-TOF-MS	12–9/06/2017 (R)	Gomez et al. (2019)
Agricultural soil	0–200	n.a.	Cfb	Field /REA-EC/PTR-MS	Summer	Schade and Custer (2004)

Notes: [a] The annotation xx ± yy denotes the mean of emission or biomass ± its standard deviation, and the formalism xx ~ yy denotes the range of emission or biomass. [b] Dfb is warm-summer humid continental climate and Cfb is temperate oceanic climate according to the World Map of Köppen-Geiger climate classification (Kottek et al., 2006). [c] DEC-MS: disjunct eddy covariance by mass scanning technique; PTR-MS: proton transfer reaction - mass spectrometry; PTR-TOF-MS: proton transfer reaction - "time-of-flight" - mass spectrometer; REA-EC: relaxed eddy accumulation - eddy covariance.

both Bachy et al. (2020) and the present study. Notably, bi-directional exchanges of methanol, including emission, uptake, and deposition, occur simultaneously on surfaces of the crop canopy and the soil. This may lead to negative fluxes under dark, wet, and cold conditions or augmented emission from the soils under light, dry, and warm conditions (Bachy et al., 2020; Bachy et al., 2016; Mozaffar, 2017; Schade and Custer, 2004). Thus, Bachy et al. (2020) have identified negative fluxes corresponding to these conditions, while neither Gomez et al. (2019) nor the present study considers the methanol sink phenomenon, and thus negative fluxes are not observed.

The large uncertainty in methanol emissions is observed in the present study, which is similar to that reported by Smiatek and Bogacki (2005) with respect to the estimation of OVOC emissions from forests in Poland (they used a semi-empirical BVOC model). The sensitivity analysis suggests that methanol emissions show a Gamma probabilistic distribution, and growth length, air temperature, solar radiation and leafage are the most important influencing variables. However, Zheng et al. (2010) found emission factor (ε), foliar density (D_m), and β-factor rather than temperature to be important sources of uncertainty in the estimation of OVOC emissions in the Pearl River Delta Metropolitan Region of China. Compared to the former two models, Zheng et al. (2010) comparatively introduced fewer model input parameters and hourly observed meteorological data to estimate regional OVOC emissions. This demonstrates that meteorological data that are more precise than what are currently on hand, especially T_{mean} and R_s, may help reduce uncertainty in estimating dynamic methanol emissions. Moreover, according to the results shown as Table S3, Fig. 4, and Fig. 5, GL, T_1, T_0, and LUE_{max} are closely related to photosynthetic period and efficiency, which, in turn, affect leaf biomass directly and methanol production indirectly, and γ_A, K, T_{opt}, and E_{opt} directly affect the production and emission of leaf methanol. Thus, more robust biomass and emission parameters are required that consider specific wheat subspecies, climate zones, and wheat phenology.

4.2. Methanol emissions affected by climate change

The warming and drought brought by the global climate change will alter methanol emissions depending on the doses and timing of

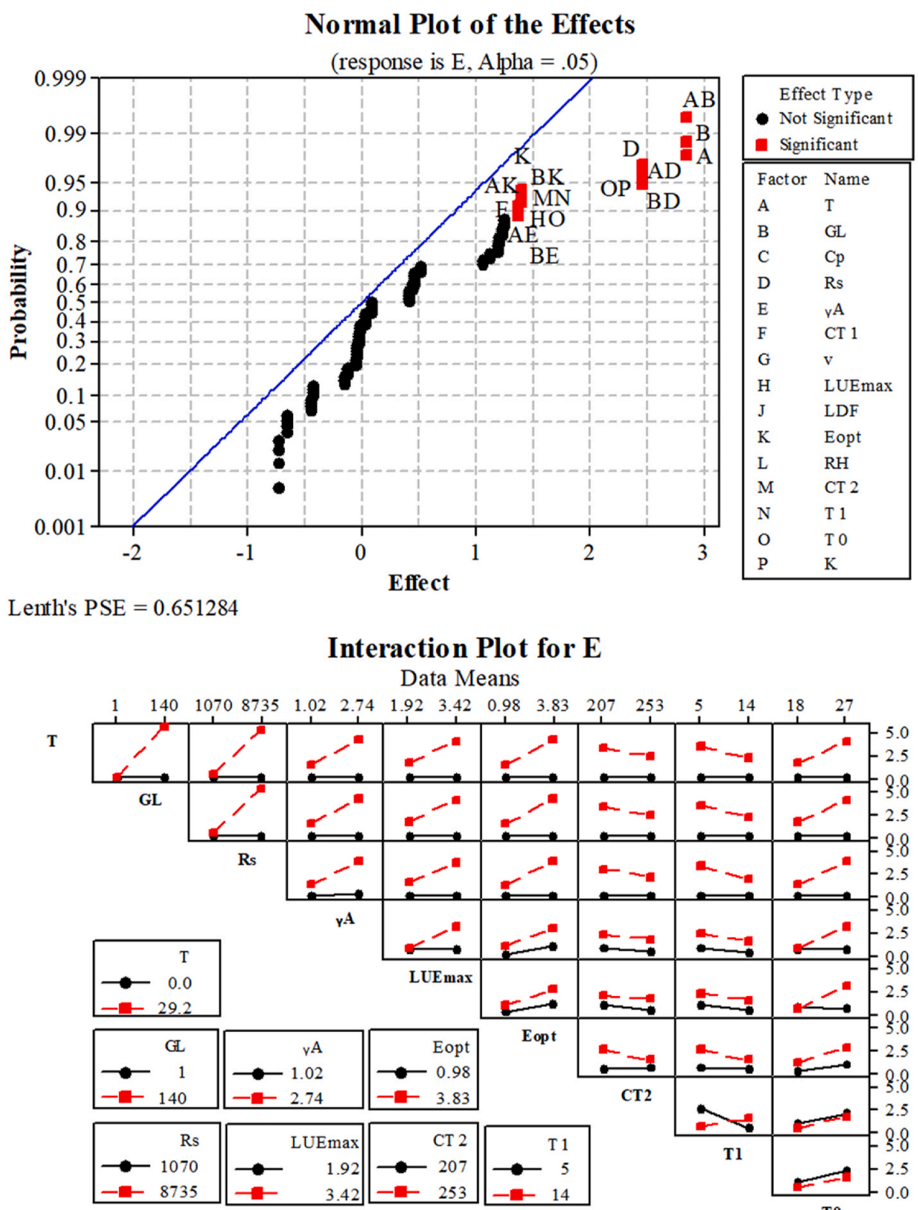

Fig. 4. Normal and interaction plots of the effects for methanol emissions considering both input data and model parameters using Minitab 16.0.

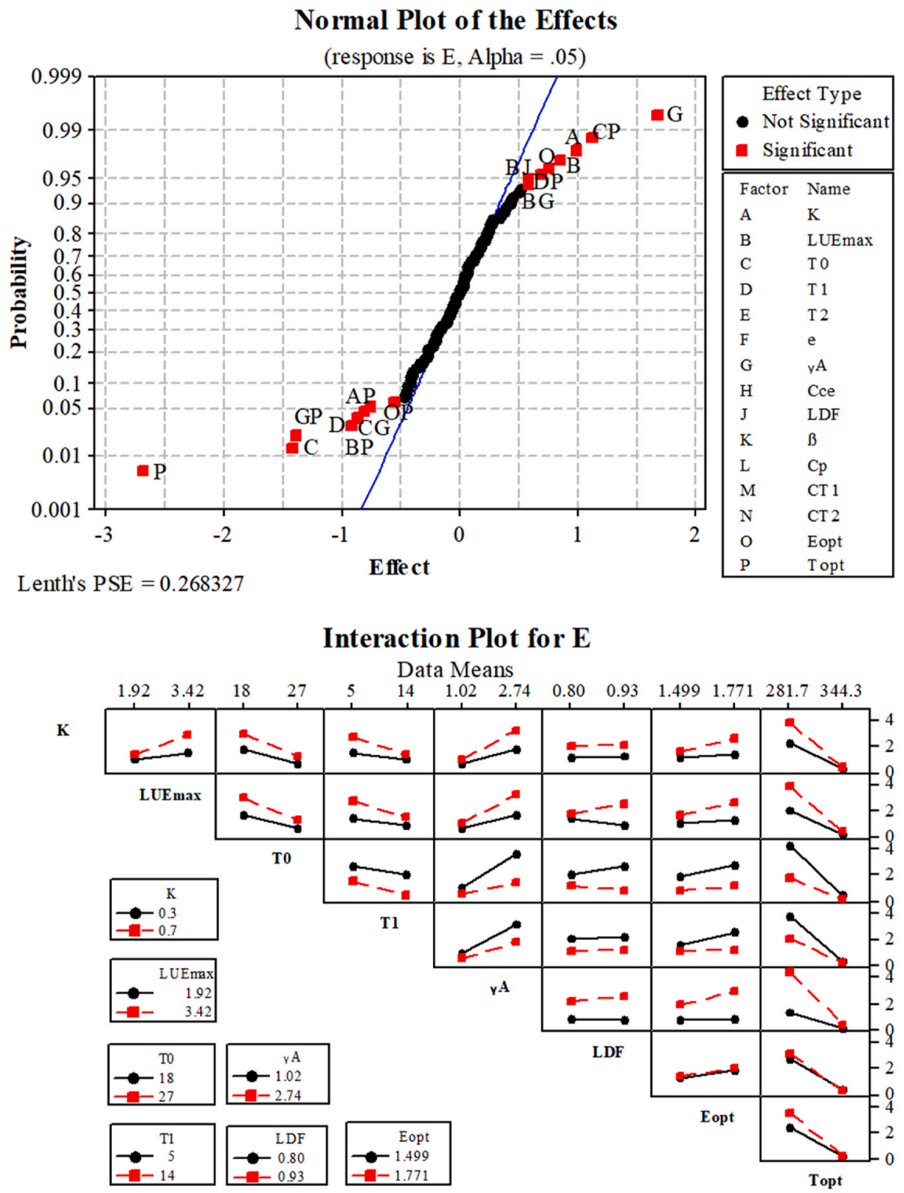

Fig. 5. Normal and interaction plots of the effects for methanol emissions only considering model parameters using Minitab 16.0.

environmental factors (Penuelas and Staudt, 2010). Considering that *P* and *RH* have not been identified as significant influencing factors (Fig. 4 and Fig. 5), only the effect of future temperature change on methanol emissions is discussed here. Temperature can strengthen the synthetase activity, lift the methanol vapor pressure, reduce the diffusion resistance, and consequently increase methanol emissions exponentially (Galbally and Kirstine, 2002). In most cases, methanol emissions increase with air temperature within a certain temperature range of 5–35 °C in the short- or medium-term, as per Fig. 1, Fig. 2, Fig. S2, and Table S2. Harley et al. (2007) have reported that each 10 °C increase in leaf temperature may cause methanol emissions to increase by as much as 2.4 times. However, enzyme degradation and physiologic responses to heat stress will also influence the emission pattern. In some cases, increasing temperatures may result in decreased or even inactivated enzyme activity (Feng et al., 2019). Stored volatiles, including methanol, can be emitted when the cell walls of the storage pools become seriously damaged at temperatures >45 °C (Guidolotti et al., 2019). Accordingly, wounding induced by excessive temperatures may strongly increase instantaneous methanol emissions.

In the long term, VOC emissions could increase with climate change due to its direct effect of warming and indirect effects on growing length, plant biomass, and vegetation composition (Lindwall et al., 2016). In the present study, there is no reduction of air temperature (Fig. S2), wheat biomass (Fig. S3), and methanol emissions (Fig. 6) in most crop districts in 2040–2069 and 2070–2099 compared to 2018. Compared to warmer southern regions in Saskatchewan, higher increases in both air temperature and wheat biomass are projected to occur in colder crop districts, e.g., D16 and D17, resulting in larger increases in emissions there. Previous studies have reported that projected climate change in 2040–2069 might cause higher grain yield, earlier seeding dates, and shorter maximum growing length (MGL) in Saskatchewan compared to the period of 1961–1990 (He et al., 2012). Crops in the southwest of Saskatchewan have earlier seeding dates and shorter MGL in most scenarios, but northeast districts have higher potential of MGL reduction in 2041–2070 compared to the baseline period of 1971–2000 (Qian et al., 2016). Thus, the projected temperature change probably causes spatial-temporal differences in the MGL of spring wheat, consequently affecting long-term methanol emission.

Although few studies have focused on long-term methanol emissions of spring wheat, studies about BVOC emissions including isoprene or

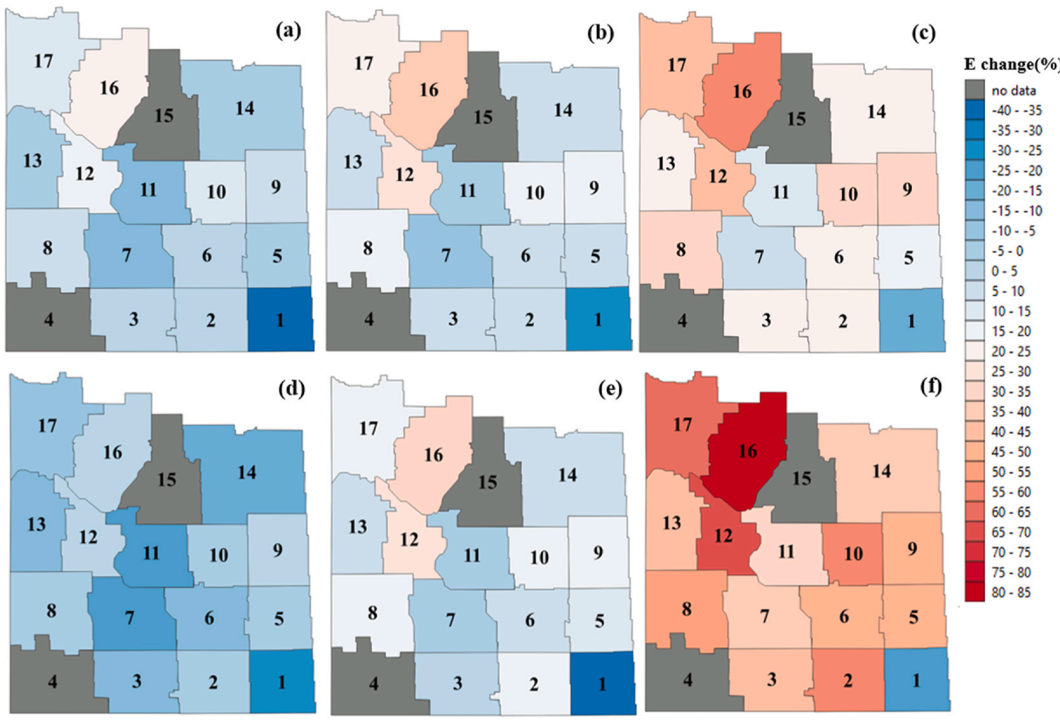

Fig. 6. Relative differences in methanol emissions (*E*, %) between 2018 observation and three periods under two SSP scenarios. (a) SSP2-4.5 scenario during 2020–2039; (b) SSP2-4.5 scenario during 2040–2069; (c) SSP2-4.5 scenario during 2070–2099; (d) SSP5-8.5 scenario during 2020–2039; (e) SSP5-8.5 scenario during 2040–2069; (f) SSP5-8.5 scenario during 2070–2099.

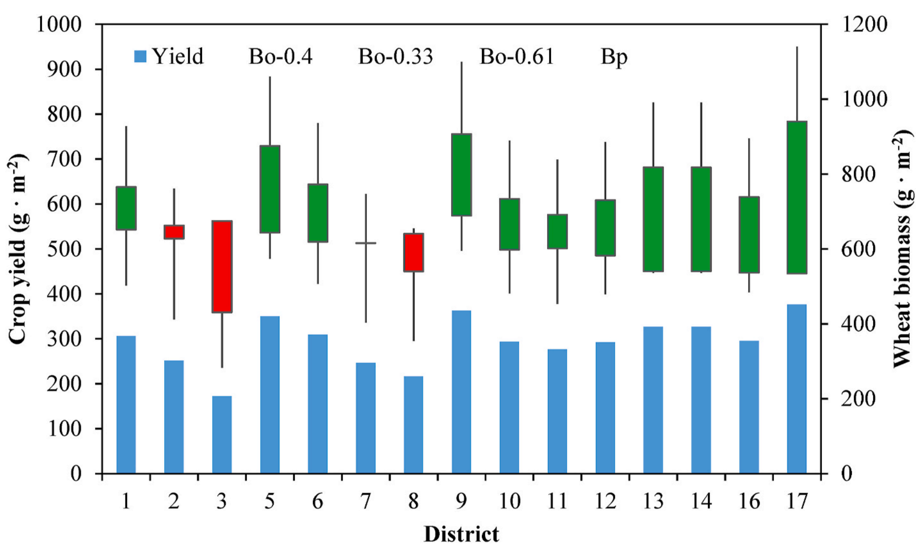

Fig. 7. The stock chart for comparison of predicted biomass (g·m^{-2}) of spring wheat from different studies. Yield (blue column) means observed crop yield of spring wheat in 2018 (Government of Saskatchewan, 2018). $B_{o\text{-}0.4}$, $B_{o\text{-}0.33}$, and $B_{o\text{-}0.61}$ mean the calculated wheat biomass using Equation (3) when the*HI* is 0.4 for spring wheat in Canada (Bolinder et al., 2007) and varies from 0.33 to 0.61 for five classes of wheat in North America (Dai et al., 2016). B_p is the predicted wheat biomass in this study. The red column represents that B_p is more than $B_{o\text{-}0.4}$ while green on the contrary. (For interpretation of the references to colour in this figure legend, the reader is referred to the Web version of this article.)

monoterpene could provide relevant comparisons. Guenther et al. (1995) estimated that a rise of 2 °C increased global BVOC emissions by 25%. Feng et al. (2019) found that warming significantly increased the emissions of isoprene (a 22% increase by +6.6 °C) and monoterpenes (a 39% increase by +1.7 °C). In general, cold zones are associated with a higher increase in air temperature compared to the global average. For example, Subarctic and Arctic areas could have an increase in air temperature at twice the global mean rate (Huang et al., 2015). Thus, BVOC emissions in cold zones may increase more than the global mean level in response to climate warming. For example, 1.9–2.5 °C rise in air temperature resulted in a doubling of emissions of monoterpenes (MTs) and sesquiterpenes (SQTs) from a wet subarctic tundra heath (Faubert et al., 2010). 2 °C warming caused 2-fold and 5-fold increases in emissions of MTs and SQTs, respectively, in northern Sweden (Valolahti et al., 2015). Notably, warming-caused increases in plant emissions cannot be fully attributed to leaf biomass because direct effects were more significant than indirect effects (Kramshøj et al., 2016; Rinnan et al., 2020). Previous studies have found that temperature—given its influence on vegetation coverage—is the primary driver of seasonal and inter-annual changes in BVOC emissions (Wang et al., 2016). For example, BVOC emissions might adapt to 3-year warming and barely change in the next decade (Tang et al., 2018). Therefore, the higher increase of methanol emissions in colder northwestern Saskatchewan is probably due to the larger temperature increases compared to that in the warmer south-eastern region.

4.3. The effect of leaf development on methanol emissions

In addition to meteorological factors such as T_{mean} and R_s, γ_A is an important factor influencing methanol emissions, as per Fig. 1, Fig. 2, Fig. 4, Fig. 5, and Fig. S2. In the present study, γ_A values of 1.02 and 2.74 are respectively assigned to stages *G–F* and *YF–R* in the updated model for spring wheat, as per Bachy et al. (2020). Accordingly, methanol emissions are predicted to be highest in the Y stage and lowest in the G stage. The emission intensity and pattern of biogenic methanol, it should be noted, depend on plant development. Leaf methanol is typically produced through pectin biosynthesis during cell wall growth and expansion, leading to the highest biogenic methanol emissions being observed in spring and early summer at both the individual and local scales (Fall and Benson, 1996; Galbally and Kirstine, 2002; Hu et al., 2011). It has also been reported that plant leaves during adulthood and during the harvesting period emit methanol at a rate several times higher than leaves during the growing period (Brunner et al., 2007; Huve et al., 2007). Notably, Mozaffar (2017) conducted a study in which strong emission peaks and guttation droplets were observed from young wheat plants following light/dark transitions, while no methanol increases or guttation droplets were found in mature plants. Moreover, as demonstrated by Oikawa et al. (2011), PME activity is expected to decrease with leaf development, and the degree of methyl esterification is known to be lower in mature cell walls than in immature leaves; as such, mature leaves have a lower potential for methanol production via the PME pathway compared to young leaves. Furthermore, a substantial proportion of methanol production in deciduous trees with mature leaves is produced in pectin demethylation during root or stem growth and transported to stomata by the transpiration stream (Folkers et al., 2008). On the other hand, Oikawa et al. (2011) demonstrated in a similar study that root methanol production is not the dominant contributor to daytime methanol emissions from mature and immature leaves of tomato plants. Interestingly, methanol emissions may be affected by inducible factors such as mechanical wounding, herbivore attacks, fungal infection, and senescence (Harrison et al., 2013). For instance, several recent studies have found that senescence-induced methanol is emitted from herbaceous plants with yellow and dry leaves (Bachy et al., 2018; 2020; Gomez et al., 2019; Mozaffar, 2017). These studies have observed strong increases in methanol emissions from wheat leaves during ear formation, fruiting, and early senescence and from maize leaves with leaf chlorosis. These observations suggest that PME and guttation could be the major pathways of biogenic methanol for immature leaves, while induced emission of methanol produced and stored in root and leaves may be the principal emission sources in mature spring wheat leaves.

4.4. The fate of biogenic methanol emissions over rural croplands

The methanol produced by plants has several fates. It can be stored in water and tissue within the plant, diffuse out through stomata to the atmosphere, or be oxidized to HCHO by the gas-phase reaction. BVOC–NO_x interaction generates highly chemically active species such as •OH and nitrate radical (NO_3), which, in turn, are responsible for the formation of pollutants such as O_3 and peroxyacetyl nitrate (PAN) (Margarita et al., 2013). Presumably, a portion of the methanol within the leaves will be ultimately converted to CO_2 (Galbally and Kirstine, 2002).

In the present study, the seasonality of methanol emissions is found to be positively correlated to concentrations of CO ($r = 0.176$, $p = 0.037$), filterable particulate matter (FPM, $r = 0.205$, $p = 0.015$), and PM_{10} ($r = 0.345$, $p < 0.001$) but negatively related to NO_2 ($r = -0.204$, $p = 0.016$) and O_3 ($r = -0.506$, $p < 0.001$), as per Fig. S5 and Table 2. However, it has been estimated that global methanol emission could produce an increase of approximately 1–2% in O_3, a 1–3% decrease in •OH, a 3–5% increase in HO_2, and a 3–9% increase in HCHO (Tie et al., 2003). The differences in O_3 formation between the two studies may be related to the sensitivity of O_3 formation to NO_x and VOCs in environments with different concentrations of anthropogenic pollutants (Vermeuel et al., 2019). O_3 formation over highly polluted urban areas is strongly VOC-sensitive and progresses towards a more NO_x-sensitive regime when the plume transports to suburban and rural areas. Limited NO_x with long-distance transport from urban areas or released by local anthropogenic activities may result in a high relative ratio of rural biogenic VOCs/NO_x, thereby maintaining •OH rather than contributing to chemical O_3 production (Jeon et al., 2014; MacKenzie et al., 2011). Moreover, the O_3 uptake by plants and soils in rural croplands and the destruction of the ozone by terpene emissions during nighttime might reduce O_3 concentrations (Im et al., 2011). Besides anthropogenic sources, VOC oxidation also contributes to CO in the atmosphere. When methanol is oxidized by •OH, HCHO and CO are sequentially produced with essentially equal yield (Hu et al., 2011). Wells et al. (2014) found that methanol explains more than 25% of the photochemical source of HCHO and CO in the north temperate zone in spring and accounts for 6% of global SOA annually. The positive relationship between methanol emissions and CO concentration was also noted by Hu et al. (2011). For instance, when methanol emissions are high in the early growing season, the large contribution to tropospheric CO and HCHO (~20%) has been observed because of a pronounced photochemical role in this period.

Table 2
Spearman's correlation of the simulated methanol emissions and the observed concentrations of six common air pollutants among District 6, 8, and 11 in 2018.

Correlation (Sig.)	Methanol	CO	FPM	NO_2	NO	NO_x	O_3	PM_{10}	SO_2
Methanol	1.000	0.176*	0.205*	−0.204*	0.092	−0.116	−0.506**	0.345**	0.044
	–	(0.037)	(0.015)	(0.016)	(0.280)	(0.173)	(0.000)	(0.000)	(0.607)
CO	0.176*	1.000	0.749**	0.681**	0.336**	0.630**	0.118	0.574**	0.527**
	(0.037)	–	(0.000)	(0.000)	(0.000)	(0.000)	(0.164)	(0.000)	(0.000)
FPM	0.205*	0.749**	1.000	0.488**	0.000	0.332**	0.355**	0.557**	0.515**
	(0.015)	(0.000)	–	(0.000)	(0.995)	(0.000)	(0.000)	(0.000)	(0.000)
NO_2	−0.204*	0.681**	0.488**	1.000	0.532**	0.928**	0.338**	0.383**	0.479**
	(0.016)	(0.000)	(0.000)	–	(0.000)	(0.000)	(0.000)	(0.000)	(0.000)
NO	0.092	0.336**	0.000	0.532**	1.000	0.778**	−0.309**	0.223**	0.208*
	(0.280)	(0.000)	(0.995)	(0.000)	–	(0.000)	(0.000)	(0.008)	(0.014)
NO_x	−0.116	0.630**	0.332**	0.928**	0.778**	1.000	0.110	0.345**	0.421**
	(0.173)	(0.000)	(0.000)	(0.000)	(0.000)	–	(0.196)	(0.000)	(0.000)
O_3	−0.506**	0.118	0.355**	0.338**	−0.309**	0.110	1.000	0.026	0.323**
	(0.000)	(0.164)	(0.000)	(0.000)	(0.000)	(0.196)	–	(0.756)	(0.000)
PM_{10}	0.345**	0.574**	0.557**	0.383**	0.223**	0.345**	0.026	1.000	0.545**
	(0.000)	(0.000)	(0.000)	(0.000)	(0.008)	(0.000)	(0.756)	–	(0.000)
SO_2	0.044	0.527**	0.515**	0.479**	0.208*	0.421**	0.323**	0.545**	1.000
	(0.607)	(0.000)	(0.000)	(0.000)	(0.014)	(0.000)	(0.000)	(0.000)	–

Notes: *. Correlation is significant at the 0.05 level (2-tailed). **. Correlation is significant at the 0.01 level (2-tailed). CO: carbon monoxide; FPM: filterable particulate matter; NO_2: nitrogen dioxide; NO: nitrogen monoxide; NO_x: $^{\text{nitrogen oxides}}$; O_3: ozone; PM_{10}: coarse particulate matter; SO_2: sulfur dioxide.

Our results have found that FPM and PM_{10} both exhibit significant positive relationships with CO, SO_2, NO_2, and NO_x concentrations (Fig. S5 and Table 2). Previous studies have reported that BVOCs can produce SOA and PM via different formation pathways, e.g., gas-phase reactions and aqueous-phase oxidation. For instance, organosulfates can be produced by nitrates and organic peroxides via gas-phase partitioning into particle-phase (Pratt et al., 2013). Sulfates and organic aerosol are responsible for most of the change in $PM_{2.5}$ concentrations (Day and Pandis, 2015). However, although methanol emissions may increase CO and PM concentrations, they have little impact on the concentrations of SO_2, NO, and NO_x ($|r| < 0.15$, $p > 0.05$) (Fig. S5 and Table 2). This means that methanol might have another pathway to produce PM rather than gas-phase reactions with nitrates and sulfates. This assumption is supported by the findings of Hansel et al. (2015). The isoprenoid photochemical oxidation will enhance the formation of sulfate and SOA, and further promote the formation and growth of new particles. However, biogenic methanol is more likely to partition into aqueous-phases—i.e., mist, fog, rain, and dew—and be oxidized by •OH. Besides, the addition reactions—e.g., dimerization, the addition reaction of hydroxyl functional groups and oxygen—will promote these aqueous-phase reactions to produce derivatives with lower vapor pressures, higher polarity, and larger molecular weights, and eventually form SOA after droplet evaporation.

4.5. Limitations and uncertainties

Besides the sources of uncertainty considered in the uncertainty and sensitivity analysis, there are still some other factors influencing methanol modeling. First, the seeding and harvesting periods vary slightly among different crop districts in the present study, and thus the classification of growth length and growing stages may increase the uncertainty of spatial-temporal simulations. Second, the effects of CO_2 and inducible stress (wounding, etc.) on methanol emissions are not incorporated in the present study. This means that the long-term constitutive methanol emissions due to the CO_2 fertilization effect on wheat biomass as well as short-term induced-methanol emissions may have been underestimated. Third, the effects of O_3 are not incorporated in the present study. Previous studies have found that the short-term exposure to O_3 rapidly reduced the SQTs (Li and Blande, 2015), the effect of O_3 on BVOC emissions varies over seasons (Yu and Blande, 2021), and the long-term exposure of O_3 to vegetation degraded yearly GPP (by about 22%) and LAI (by 15–20%) (Anav et al., 2011). Therefore, the effects of O_3 on methanol emissions are unclear and it should be an important consideration in future work. Fourth, although standard emission factor (ε) is not identified as $SF_{<0.05}$ because of its smaller range compared to other factors, the use of a constant ε for common wheat (winter wheat) at the ripening stage to represent spring wheat throughout the whole growing period (which was done due to the lack of experimental data) may increase uncertainty concerning the base methanol emissions calculated. Thus, in future work the missing environmental and physicochemical factors should be included in the development of empirical algorithms through more field and laboratory measurements of methanol emissions for specific wheat subspecies, climate zones, and wheat phenologies. Fifth, in the present study the bias correction is calculated using daily observed and control run temperature in 2018. Using long-term climate data to correct the bias of projected temperature might increase the accuracy of the bias-corrected temperature that is used to drive the methanol emission model. Sixth, methanol emission is estimated by district rather than by grid. Remote Sensing (RS) and Geospatial Information Systems (GIS) can be further combined to provide cropland area, LAI, and foliar densities, meteorological data, etc. Compared to ground station data, these interpretative data of RS images can be used to estimate the gridded methanol emissions with a finer spatial-temporal resolution and to quantify the impact of continuous methanol emission changes on air pollution along the surface (Xiao et al., 2020). Finally, soils and litter are also significant contributors to methanol emissions (Bachy et al., 2018). For instance, it has been found that methanol could account for 28–99% of total VOC emissions from decomposing litterfalls (Gray and Fierer, 2012). Methanol fluxes from bare and plowed soil could range from 0 to 200 $\mu g \cdot m^{-2} \cdot h^{-1}$ (Schade and Custer, 2004). The large differences in methanol emissions may result from N additions, warming, wildfire, and drainage conditions in soils (Huang et al., 2020; Kramshøj et al., 2019; Zhang-Turpeinen et al., 2020). However, only leaf methanol is calculated in the present study, and several additional methanol sources could be considered in future work, such as above-ground fruits and flowers, the shedding of leaves and stems on the surface, underground living roots, microbial decomposition of litter and SOM, dissolved methanol in soil water, methanol exchange in soil–plant–atmosphere ecosystems (Cai et al., 2020; Chen et al., 2020; Feng et al., 2020).

5. Conclusions

In this study, methanol emissions from spring wheat during the growing period were estimated using a developed emission model. The temporal and spatial variations of methanol emissions of spring wheat in Saskatchewan were investigated. The averaged methanol emission of spring wheat is found to be 37.94 ± 7.5 $\mu g \cdot m^{-2} \cdot h^{-1}$, increasing from north to south and exhibiting phenological peak to valley characteristics. Moreover, cold crop districts are projected to be with higher increase in air temperature and consequent methanol emissions during 2020–2099. Furthermore, the seasonality of methanol emissions is found to be positively correlated to concentrations of CO, FPM, and PM_{10} but negatively related to NO_2 and O_3. The uncertainty and sensitivity analysis results suggest that methanol emissions show a Gamma probabilistic distribution. Growth length, air temperature, solar radiation, and leafage are the most important influencing variables. In most cases, methanol emissions increase with air temperature in the range of 3–35 °C while the excessive temperature may result in decreased methanol emissions because of inactivated enzyme activity or increased instant methanol emissions due to heat injury. Notably, induced emission might be the major source of biogenic methanol of mature leaves. The results of this study can be used to develop appropriate strategies for regional emission management of cropping systems.

Author contributions

Mengfan Cai: Conceived and designed the analysis, Collected the data, Performed the analysis, Wrote the paper. *Chunjiang An:* Conceived and designed the analysis, Performed the analysis, Other contribution. *Christophe Guy:* Conceived and designed the analysis, Other contribution. *Chen Lu:* Conceived and designed the analysis, Other contribution. *Fereshteh Mafakheri:* Other contribution.

Declaration of competing interest

The authors declare that they have no known competing financial interests or personal relationships that could have appeared to influence the work reported in this paper.

Acknowledgements

This research was supported by the Natural Sciences and Engineering Research Council of Canada (NSERC). The authors are grateful to the editor and anonymous reviewers for their insightful comments and suggestions. The first author, Mengfan Cai, commemorates the *Father of Hybrid Rice*, Longping Yuan (September 7, 1930–May 22, 2021), for his huge contribution and great inspiration.

Appendix A. Supplementary data

Supplementary data to this article can be found online at https://doi.

org/10.1016/j.envpol.2021.117602.

References

Albrizio, R., Steduto, P., 2003. Photosynthesis, respiration and conservative carbon use efficiency of four field grown crops. Agric. For. Meteorol. 116, 19–36.

Anav, A., Menut, L., Khvorostyanov, D., et al., 2011. Impact of tropospheric ozone on the Euro-Mediterranean vegetation. Global Change Biol. 17, 2342–2359.

Asif, Z., Chen, Z., 2020. A life cycle based air quality modeling and decision support system (LCAQMS) for sustainable mining management. J. Environ. Info. 35 (2), 103–117.

Bachy, A., Aubinet, M., Amelynck, C., et al., 2020. Dynamics and mechanisms of volatile organic compound exchanges in a winter wheat field. Atmos. Environ. 221, 117105.

Bachy, A., Aubinet, M., Amelynck, C., et al., 2018. Methanol exchange dynamics between a temperate cropland soil and the atmosphere. Atmos. Environ. 176, 229–239. https://doi.org/10.1016/j.atmosenv.2017.12.016.

Bachy, A., Aubinet, M., Schoon, N., et al., 2016. Are BVOC exchanges in agricultural ecosystems overestimated? Insights from fluxes measured in a maize field over a whole growing season. Atmos. Chem. Phys. 16, 5343–5356. https://doi.org/10.5194/acp-16-5343-2016.

Bolinder, M.A., Janzen, H.H., Gregorich, E.G., et al., 2007. An approach for estimating net primary productivity and annual carbon inputs to soil for common agricultural crops in Canada. Agric. Ecosyst. Environ. 118, 29–42. https://doi.org/10.1016/j.agee.2006.05.013.

Brunner, A., Ammann, C., Neftel, A., et al., 2007. Methanol exchange between grassland and the atmosphere. Biogeosciences 4, 395–410. https://doi.org/10.5194/bg-4-395-2007.

Cai, M., An, C., Guy, C., et al., 2020. Assessment of soil and water conservation practices in the loess hilly region using a coupled rainfall-runoff-erosion model. Sustainability 12, 934. https://doi.org/10.3390/su12030934.

Cai, M., An, C., Guy, C., 2021. A scientometric analysis and review of biogenic volatile organic compound emissions: research hotspots, new frontiers, and environmental implications. Renew. Sustain. Energy Rev. https://doi.org/10.1016/j.rser.2021.111317. In press.

Cai, M., Xin, Z., Yu, X., 2017. Spatio-temporal variations in PM leaf deposition: a meta-analysis. Environ. Pollut. 231, 207–218.

Cai, M., Xin, Z., Yu, X., 2019. Particulate matter transported from urban greening plants during precipitation events in Beijing, China. Environ. Pollut. 252, 1648–1658.

Caravan, R.L., Khan, M.A.H., Zádor, J., et al., 2018. The reaction of hydroxyl and methylperoxy radicals is not a major source of atmospheric methanol. Nat. Commun. 9, 1–9.

Chen, Z., An, C., Fang, H., et al., 2020. Assessment of regional greenhouse gas emission from beef cattle production: a case study of Saskatchewan in Canada. J. Environ. Manag. 264, 110443.

Collalti, A., Tjoelker, M.G., Hoch, G., et al., 2020. Plant respiration: controlled by photosynthesis or biomass? Global Change Biol. 26, 1739–1753.

Custer, T., Schade, G., 2007. Methanol and acetaldehyde fluxes over ryegrass. Tellus Ser. B Chem. Phys. Meteorol. 59, 673–684. https://doi.org/10.1111/j.1600-0889.2007.00294.x.

Dai, J., Bean, B., Brown, B., et al., 2016. Harvest index and straw yield of five classes of wheat. Biomass Bioenergy 85, 223–227. https://doi.org/10.1016/j.biombioe.2015.12.023.

Day, M.C., Pandis, S.N., 2015. Effects of a changing climate on summertime fine particulate matter levels in the eastern US. J. Geophys. Res.-Atmos. 120, 5706–5720. https://doi.org/10.1002/2014jd022889.

Eyring, V., Bony, S., Meehl, G.A., et al., 2016. Overview of the coupled model intercomparison project phase 6 (CMIP6) experimental design and organization. Geosci. Model Dev. (GMD) 9, 1937–1958.

Fall, R., Benson, A.A., 1996. Leaf methanol—the simplest natural product from plants. Trends Plant Sci. 1, 296–301.

FAO, 2018. Crops Data from Food and Agriculture Organization of the United Nations (FAO). Available via. http://www.fao.org/faostat/en/?#data/QC. (Accessed 2 June 2021).

Faubert, P., Tiiva, P., Rinnan, A., et al., 2010. Doubled volatile organic compound emissions from subarctic tundra under simulated climate warming. New Phytol. 187, 199–208. https://doi.org/10.1111/j.1469-8137.2010.03270.x.

Feng, Q., An, C., Chen, Z., et al., 2020. Can deep tillage enhance carbon sequestration in soils? A meta-analysis towards GHG mitigation and sustainable agricultural management. Renew. Sustain. Energy Rev. 133, 110293.

Feng, Z.Z., Yuan, X.Y., Fares, S., et al., 2019. Isoprene is more affected by climate drivers than monoterpenes: a meta-analytic review on plant isoprenoid emissions. Plant Cell Environ. 42, 1939–1949. https://doi.org/10.1111/pce.13535.

Folkers, A., Hüve, K., Ammann, C., et al., 2008. Methanol emissions from deciduous tree species: dependence on temperature and light intensity. Plant Biol. 10, 65–75.

Galbally, I.E., Kirstine, W., 2002. The production of methanol by flowering plants and the global cycle of methanol. J. Atmos. Chem. 43, 195–229.

Gomez, L.G., Loubet, B., Lafouge, F., et al., 2019. Comparative study of biogenic volatile organic compounds fluxes by wheat, maize and rapeseed with dynamic chambers over a short period in northern France. Atmos. Environ. 214, 16. https://doi.org/10.1016/j.atmosenv.2019.116855.

Government of Canada, 2016. Canadian Weather Energy and Engineering Datasets (CWEEDS2016). Available via. https://climate.weather.gc.ca/prods_servs/engineering_e.html. (Accessed 2 June 2021).

Government of Canada, 2018. 2018 Crop Reports. Available via. https://publications.saskatchewan.ca/#/categories/2629. (Accessed 2 June 2021).

Government of Saskatchewan, 2018. Historical Data. Available via. https://climate.weather.gc.ca/historical_data/search_historic_data_e.html. (Accessed 2 June 2021).

Gower, S.T., Kucharik, C.J., Norman, J.M., 1999. Direct and indirect estimation of leaf area index, fAPAR, and net primary production of terrestrial ecosystems. Rem. Sens. Environ. 70, 29–51.

Gray, C.M., Fierer, N., 2012. Impacts of nitrogen fertilization on volatile organic compound emissions from decomposing plant litter. Global Change Biol. 18, 739–748.

Guenther, A., Hewitt, C.N., Erickson, D., et al., 1995. A global model of natural volatile organic compound emissions. J. Geophys. Res.: Atmos. 100, 8873–8892.

Guenther, A., Karl, T., Harley, P., et al., 2006. Estimates of global terrestrial isoprene emissions using MEGAN (model of emissions of gases and aerosols from nature). Atmos. Chem. Phys. 6, 3181–3210. https://doi.org/10.5194/acp-6-3181-2006.

Guenther, A.B., Jiang, X., Heald, C.L., et al., 2012. The model of emissions of gases and aerosols from nature version 2.1 (MEGAN2.1): an extended and updated framework for modeling biogenic emissions. Geosci. Model Dev. (GMD) 5, 1471–1492. https://doi.org/10.5194/gmd-5-1471-2012.

Guidolotti, G., Pallozzi, E., Gavrichkova, O., et al., 2019. Emission of constitutive isoprene, induced monoterpenes, and other volatiles under high temperatures in Eucalyptus camaldulensis: a C-13 labelling study. Plant Cell Environ. 42, 1929–1938. https://doi.org/10.1111/pce.13521.

Hansel, A.K., Ehrenhauser, F.S., Richards-Henderson, N.K., et al., 2015. Aqueous-phase oxidation of green leaf volatiles by hydroxyl radical as a source of SOA: product identification from methyl jasmonate and methyl salicylate oxidation. Atmos. Environ. 102, 43–51. https://doi.org/10.1016/j.atmosenv.2014.11.055.

Harley, P., Greenberg, J., Niinemets, Ü., et al., 2007. Environmental Controls over Methanol Emission from Leaves.

Harrison, S.P., Morfopoulos, C., Dani, K.S., et al., 2013. Volatile isoprenoid emissions from plastid to planet. New Phytol. 197, 49–57.

He, M., Kimball, J.S., Maneta, M.P., et al., 2018. Regional crop gross primary productivity and yield estimation using fused landsat-MODIS data. Rem. Sens. 10, 372.

He, Y., Wang, H., Qian, B., et al., 2012. How early can the seeding dates of spring wheat be under current and future climate in Saskatchewan, Canada? PloS One 7, e45153.

Heikes, B.G., Chang, W.N., Pilson, M.E.Q., et al., 2002. Atmospheric methanol budget and ocean implication. Global Biogeochem. Cycles 16, 13. https://doi.org/10.1029/2002gb001895.

Hu, L., Millet, D.B., Mohr, M.J., et al., 2011. Sources and seasonality of atmospheric methanol based on tall tower measurements in the US Upper Midwest. Atmos. Chem. Phys. 11, 11145–11156. https://doi.org/10.5194/acp-11-11145-2011.

Huang, L., McDonald-Buller, E., McGaughey, G., et al., 2015. Comparison of regional and global land cover products and the implications for biogenic emission modeling. J. Air Waste Manag. Assoc. 65, 1194–1205. https://doi.org/10.1080/10962247.2015.1057302.

Huang, X., Lai, J., Liu, Y., et al., 2020. Biogenic volatile organic compound emissions from Pinus massoniana and Schima superba seedlings: their responses to foliar and soil application of nitrogen. Sci. Total Environ. 705, 135761.

Huve, K., Christ, M.M., Kleist, E., et al., 2007. Simultaneous growth and emission measurements demonstrate an interactive control of methanol release by leaf expansion and stomata. J. Exp. Bot. 58, 1783–1793. https://doi.org/10.1093/jxb/erm038.

Im, U., Poupkou, A., Incecik, S., et al., 2011. The impact of anthropogenic and biogenic emissions on surface ozone concentrations in Istanbul. Sci. Total Environ. 409, 1255–1265. https://doi.org/10.1016/j.scitotenv.2010.12.026.

Jeon, W.B., Lee, S.H., Lee, H., et al., 2014. A study on high ozone formation mechanism associated with change of NOx/VOCs ratio at a rural area in the Korean Peninsula. Atmos. Environ. 89, 10–21. https://doi.org/10.1016/j.atmosenv.2014.02.005.

Ji, L., Huang, G., Niu, D., et al., 2020. A stochastic optimization model for carbon-emission reduction investment and sustainable energy planning under cost-risk control. J. Environ. Info. 36 (2), 107–118.

Kottek, M., Grieser, J., Beck, C., et al., 2006. World Map of the Köppen-Geiger Climate Classification Updated.

Kramshøj, M., Albers, C.N., Svendsen, S.H., et al., 2019. Volatile emissions from thawing permafrost soils are influenced by meltwater drainage conditions. Global Change Biol. 25, 1704–1716.

Kramshøj, M., Vedel-Petersen, I., Schollert, M., et al., 2016. Large increases in Arctic biogenic volatile emissions are a direct effect of warming. Nat. Geosci. 9, 349–352.

Li, T., Blande, J.D., 2015. Associational susceptibility in broccoli: mediated by plant volatiles, impeded by ozone. Global Change Biol. 21, 1993–2004.

Lindwall, F., Schollert, M., Michelsen, A., et al., 2016. Fourfold higher tundra volatile emissions due to arctic summer warming. J. Geophys. Res.-Biogeosci. 121, 895–902. https://doi.org/10.1002/2015jg003295.

MacKenzie, A.R., Langford, B., Pugh, T.A.M., et al., 2011. The atmospheric chemistry of trace gases and particulate matter emitted by different land uses in Borneo. Phil. Trans. Biol. Sci. 366, 3177–3195. https://doi.org/10.1098/rstb.2011.0053.

Maraun, D., 2016. Bias correcting climate change simulations-a critical review. Curr. Clim. Chang. Rep. 2, 211–220.

Margarita, P., Karina, C., Johanna, M., 2013. Emission factors of biogenic volatile organic compounds in various stages of growth present in the urban forest of the Metropolitan Region, Chile. Res. J. Chem. Environ. 17, 1–9.

Mozaffar, A., 2017. Exchanges of Biogenic Volatile Organic Compounds between the Atmosphere and Agricultural Plants/ecosystems in Controlled and Field Conditions. Université de Liège, Liège, Belgique.

Oikawa, P.Y., Giebel, B.M., Sternberg, L., et al., 2011. Leaf and root pectin methylesterase activity and C-13/C-12 stable isotopic ratio measurements of methanol emissions give insight into methanol production in Lycopersicon

esculentum. New Phytol. 191, 1031–1040. https://doi.org/10.1111/j.1469-8137.2011.03770.x.
Patel, N., Dadhwal, V., Saha, S., et al., 2010. Evaluation of MODIS data potential to infer water stress for wheat NPP estimation. Trop. Ecol. 51, 93.
Penuelas, J., Filella, I., Stefanescu, C., et al., 2005. Caterpillars of Euphydryas aurinia (Lepidoptera : nymphalidae) feeding on Succisa pratensis leaves induce large foliar emissions of methanol. New Phytol. 167, 851–857. https://doi.org/10.1111/j.1469-8137.2005.01459.x.
Peñuelas, J., Sardans, J., Estiarte, M., et al., 2013. Evidence of current impact of climate change on life: a walk from genes to the biosphere. Global Change Biol. 19, 2303–2338.
Penuelas, J., Staudt, M., 2010. BVOCs and global change. Trends Plant Sci. 15, 133–144. https://doi.org/10.1016/j.tplants.2009.12.005.
Pratt, K.A., Fiddler, M.N., Shepson, P.B., et al., 2013. Organosulfates in cloud water above the Ozarks' isoprene source region. Atmos. Environ. 77, 231–238. https://doi.org/10.1016/j.atmosenv.2013.05.011.
Qian, B., De Jong, R., Huffman, T., et al., 2016. Projecting yield changes of spring wheat under future climate scenarios on the Canadian Prairies. Theor. Appl. Climatol. 123, 651–669.
Rinnan, R., Iversen, L.L., Tang, J., et al., 2020. Separating direct and indirect effects of rising temperatures on biogenic volatile emissions in the Arctic. Proc. Natl. Acad. Sci. U. S. A 117, 32476–32483. https://doi.org/10.1073/pnas.2008901117.
Sánchez, M., Pardo, N., Pérez, I., et al., 2015. GPP and maximum light use efficiency estimates using different approaches over a rotating biodiesel crop. Agric. For. Meteorol. 214, 444–455.
Schade, G.W., Custer, T.G., 2004. OVOC emissions from agricultural soil in northern Germany during the 2003 European heat wave. Atmos. Environ. 38, 6105–6114.
Shi, Y., Huang, G., An, C., et al., 2021. Assessment of regional greenhouse gas emissions from spring wheat cropping system: a case study of Saskatchewan in Canada. J. Clean. Prod. 301, 126917.
Shrestha, N., Wang, J., 2020. Water quality management of a cold climate region watershed in changing climate. J. Environ. Info. 35 (1), 56–80.
Shrivastava, M., Cappa, C.D., Fan, J., et al., 2017. Recent advances in understanding secondary organic aerosol: implications for global climate forcing. Rev. Geophys. 55, 509–559.
Smiatek, G., Bogacki, M., 2005. Uncertainty assessment of potential biogenic volatile organic compound emissions from forests with the Monte Carlo method: case study for an episode from 1 to 10 July 2000 in Poland. J. Geophys. Res.: Atmos. 110.
Statistics Canada, 2021. Table 32-10-0359-01 Estimated areas, yield, production, average farm price and total farm value of principal field crops, in metric and imperial units. Available via. https://doi.org/10.25318/3210035901-eng. (Accessed 2 June 2021).
Stavrakou, T., Guenther, A., Razavi, A., et al., 2011. First space-based derivation of the global atmospheric methanol emission fluxes. Atmos. Chem. Phys. 11, 4873–4898. https://doi.org/10.5194/acp-11-4873-2011.
Tang, J., Valolahti, H., Kivimaenpaa, M., et al., 2018. Acclimation of biogenic volatile organic compound emission from subarctic heath under long-term moderate warming. J. Geophys. Res.-Biogeosci. 123, 95–105. https://doi.org/10.1002/2017jg004139.
Tie, X., Guenther, A., Holland, E., 2003. Biogenic methanol and its impacts on tropospheric oxidants. Geophys. Res. Lett. 30.
Valolahti, H., Kivimäenpää, M., Faubert, P., et al., 2015. Climate change-induced vegetation change as a driver of increased subarctic biogenic volatile organic compound emissions. Global Change Biol. 21, 3478–3488.
Vermeuel, M.P., Novak, G.A., Alwe, H.D., et al., 2019. Sensitivity of ozone production to NOx and VOC along the lake Michigan coastline. J. Geophys. Res.: Atmos. 124, 10989–11006.
Wang, H., Wang, X., Zhang, Y., et al., 2016. Evident elevation of atmospheric monoterpenes due to degradation-induced species changes in a semi-arid grassland. Sci. Total Environ. 541, 1499–1503.
Wells, K.C., Millet, D.B., Cady-Pereira, K.E., et al., 2014. Quantifying global terrestrial methanol emissions using observations from the TES satellite sensor. Atmos. Chem. Phys. 14, 2555–2570. https://doi.org/10.5194/acp-14-2555-2014.
Wu, H., Chen, J., Zeng, G., Xu, J., Sang, L., Liu, Q., Dai, J., et al., 2020. Effects of early dry season on habitat suitability for migratory birds in China's two largest freshwater lake wetlands after the impoundment of Three Gorges Dam. J. Environ. Info. 36 (2), 82–92.
Xiao, L., Christakos, G., He, J., Lang, Y., 2020. Space-time ground-level PM 2.5 distribution at the Yangtze River Delta: a comparison of Kriging, LUR, and combined BME-LUR techniques. J. Environ. Info. 36 (1), 33–42.
Yu, H., Blande, J.D., 2021. Diurnal Variation in BVOC Emission and CO_2 Gas Exchange from Above-And Belowground Parts of Two Coniferous Species and Their Responses to Elevated O_3. Environmental Pollution, p. 116830.
Zhang-Turpeinen, H., Kivimäenpää, M., Aaltonen, H., et al., 2020. Wildfire effects on BVOC emissions from boreal forest floor on permafrost soil in Siberia. Sci. Total Environ. 711, 134851.
Zheng, J., Zheng, Z., Yu, Y., et al., 2010. Temporal, spatial characteristics and uncertainty of biogenic VOC emissions in the Pearl River Delta region, China. Atmos. Environ. 44, 1960–1969.